JOURNAL OF GUIDANCE, CONTROL, AND DYNAMICS
Vol. 17, No. 2, March–April 1994

Optimal Linear Quadratic Gaussian Digital Control of an Orbiting Tethered Antenna/Reflector System

Zhaozhi Tan* and Peter M. Bainum†
Howard University, Washington, DC 20059

Analysis and design of linear quadratic Gaussian (LQG) optimal digital controllers and estimators are presented for a flexible orbiting tethered shell system. Emphasis is placed on mathematical models of the dynamics, influence of the number of actuators and their locations, methods of measurement of the state variables, and design of LQG optimal digital controllers and observers. Attitude and shape control is accomplished using point actuators and tether tension. A new practical method is presented to measure the tether transverse motion. Actuator and sensor placements are obtained by means of the concept of the degree of controllability and observability, as well as related simulations. The analysis and design of the optimal LQG digital control system for the tethered shell has been validated by simulation. After maximizing the degree of controllability and observability, the best combination of the controller and observer pole locations is found by carefully selecting the weighting matrices. Typical figures show satisfactory transient response under LQG control laws.

Nomenclature

A = area of the tether cross section
A_m, B_m, C_m = amplitudes of the longitudinal, in-plane, and out-of-plane components of the mth mode of the tether, respectively
A_{pn} = nth modal amplitude of the shell
a = base radius of the shell
D = bending stiffness of the shell
E = Young's modulus of the tether
E_n = generic force on the nth mode of the shell
E_p = $\int_p e\, dm$
E_{st} = $\int_{st} e\, dm$
e = external force acting per unit mass
F_{px} = component of the tether force acting on the shell along the shell symmetry axis
F_{tx} = tether tension
H_{ex}, H_{ey}, H_{ez} = result from the external force[1]
$H_{(.)(*)}$ = $\int_{st} (.)(*)\, dm$
$H^*_{(.)(*)}$ = $H_{(.)(*)} - I_{(.)} I_{(*)}/m_\Sigma$
h = length of the boom
$I_p(.), J_p(.)$ = modified Bessel function and Bessel function, respectively, of the first kind and order p
$I_1^{(n)}$ = $\int_p x_p \phi_{pn}\, dm$
$I_{(.)}$ = $\int_{st} (.)\, dm$
$I^*_{(.)}$ = $m_p I_{(.)}/m_\Sigma$
J_x, J_y, J_z = moment of inertia of the shell about the principal axes x, y, and z, respectively
J_y^* = $J_y + m_{st}^* h^2 + I_x^* h$
J_z^* = $J_z + m_{st}^* h^2 + I_x^* h$
j = number of the nodal circles of the shell
K_{mn} = 0, $(m \neq n)$
K_{nn} = $EA\beta_n^2(1 + m_s \sin^2\beta_n/m_t)/2L$
L = tether length
$L_{Epx}, L_{Epy}, L_{Epz}$ = components of torque, produced by E_{st} and E_p, which appear in the tether force acting on the shell[1]
$L_{epx}, L_{epy}, L_{epz}$ = components of torque contributed by the external force acting on the shell
L_{ey}, L_{ez} = torques produced by the external force
M_n = nth modal mass of the shell
m_p, m_s, m_t = masses of shell, subsatellite, and tether, respectively
m_{st} = $m_s + m_t$
m_{st}^* = $m_{st} \cdot m_p/m_\Sigma$
m_Σ = $m_p + m_s + m_t$
p = number of the nodal diameters (meridians) of the shell
R = radius of the shell's curvature
r = radial distance of a shell element from the symmetry axis
u_{po} = displacement of the shell's apex
α = tether in-plane swing angle
γ = tether out-of-plane swing angle
θ = pitch angle of the shell
ξ = r/a
ϕ_m = mth shape function of the tether transverse vibration
ϕ_{pn} = nth modal shape function of shell vibration[2], $A_{pj}[a^{p+4}C_{pj}\xi^p/(RD\lambda_{pj}^4) + J_p(\lambda_{pj}\xi) + D_{pj}I_p(\lambda_{pj}\xi)]\cos p(\beta_1 + \beta_o)$
ϕ_p^o = shape function at the shell's apex
ϕ = roll angle of the shell
ψ_m = mth shape function of the tether longitudinal vibration
ψ = yaw angle of the shell
ω_c = orbital angular velocity
ω_n = nth mode natural frequency of tether transverse vibration
ω_{pn} = shell frequency of the nth mode
$(\,)'$ = $d(\,)/d(\omega_c t)$

Presented as Paper 92-118 at the AAS/AIAA Spaceflight Mechanics Meeting, Colorado Springs, CO, Feb. 24–26, 1992; received March 29, 1992; revision received Jan. 8, 1993; accepted for publication Jan. 8, 1993.

*Visiting Research Associate, Department of Mechanical Engineering. Student Member AIAA.
†Distinguished Professor of Aerospace Engineering, Department of Mechanical Engineering. Fellow AIAA.

Introduction

SINCE the early 1970s very large space antennas have been proposed for power transmission, astronomical research, and communications. The gravity stabilized configuration is particularly suited for very large flexible systems to alleviate the problems associated with the active control of very large structures. A tethered shell structure (Fig. 1) to provide the favorable moment of inertia distribution for overall gravitational stabilization has been investigated by Liu and Bainum.[3] In their paper for a rigid shell and a flexible tether, the control problem, by using the continuous-time linear quadratic regulator technique, has been solved. Because of the large size and small mass, it is necessary for the further analysis to consider the shell to be flexible. The vibrations of the shell affect the tether motion and tension and are coupled to the rotations of the shell. To control the shapes and attitudes of the shell and the tether, tether tension alone is not enough; therefore, the addition of a few jets as point actuators is suggested. The number and location of the actuators are determined by means of the concept of the degree of controllability presented by Xing and Bainum,[4] the advantages of which are the clarity of physical and geometrical interpretations and simplicity of the resulting calculation. The state measurement is another important problem. In this paper it is shown that the system will be unobservable if the tether out-of-(orbit) plane swing motion or transverse vibration is not directly measured. A method to measure the tether transverse vibration and swing motion is developed in this paper; this method may be implemented in engineering practice and can provide a high measurement accuracy. It can be used for any orbiting tethered system. With this method and a few properly placed sensors, it is found that the system will have a satisfactory degree of observability.

In engineering practice a discrete time data system is more practical for the controller based on the on-board computer. Thus the linear quadratic Gaussian (LQG) technique (design of the optimal stochastic controller for a problem described in terms of linear system models, quadratic cost criteria, and Gaussian noise models) is employed to synthesize a controller with a Kalman filter to deal with the measurement noise and plant noise in the presence of sampled data observations.

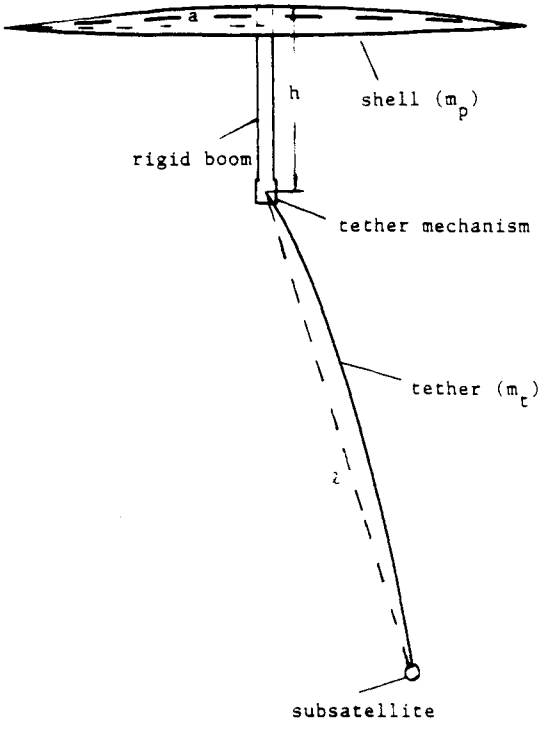

Fig. 1 Tethered antenna/reflector system.

Mathematical Model

Dynamical Equations

The mathematical model of a tethered shell system in orbit was developed in Ref. 3. The resulting linearized equations of motion were developed as follows.

1) Shell attitude:

$$\psi'' - (J_z^* - J_y^*)/J_x\psi - \left[1 + (J_z^* - J_y^*)/J_x\right]\phi' = (L_{Epx} + L_{epx})/J_x\omega_c^2 \tag{1}$$

$$\theta'' - 3(J_x - J_z^*)/J_y^*\theta - 2\sum_n I_1^{(n)}A'_{pn}/J_y^* - (h/J_y^*)\left[\sum_m I_{\phi_m}^* C_m'' + 2m_{st}^*(L' - u'_{po}) + 2\sum_m I_{\psi_m}^* A'_m - I_x^*\alpha''\right] = (L_{Epy} + L_{epy})/J_y^*\omega_c^2 \tag{2}$$

$$\phi'' + 4(J_y^* - J_x)/J_z^*\phi + \left[1 - (J_y^* - J_x)/J_z^*\right]\psi' - h\left[(\gamma'' + \gamma)I_x^* + \sum_m I_{\phi_m}^*(B_m'' + B_m)\right]\Big/J_z^* = -(L_{Epz} + L_{epz})/J_z^*\omega_c^2 \tag{3}$$

2) Tether longitude and swing motions:

$$\omega_c^2\left[m_{st}^*(L'' - u_{po}'' + 3u_{po}) + \sum_m I_{\Downarrow_m}^*(A_m'' - 3A_m) - 2\sum_m I_{\Phi_m}^* C_m' + (2\alpha' + 2\theta' - 3)I_x^* - hm_{st}^*(3 - 2\theta')\right] = F_{tx} + (m_p E_{stx} - m_{st}E_{px})/m_\Sigma \tag{4}$$

$$H_{xx}^*\alpha'' + (\theta'' + 3\alpha + 3\theta)(H_{xx}^* + hI_x^*) - \sum_m H_{x\phi_m}^* C_m'' - 3\sum_m (H_{x\phi_m}^* + hI_{\phi_m}^*)C_m - 2I_x^*(L' - u'_{po}) - 2\sum_m H_{x\psi_m}^* A'_m = L_{ey}/\omega_c^2 \tag{5}$$

$$H_{xx}^*(\gamma'' + \gamma) - (H_{xx}^* + hI_x^*)(\phi'' + 4\phi - 3\gamma) + \sum_m H_{x\phi_m}^*(B_m'' + B_m) + 3\sum_m (H_{x\phi_m}^* + hI_{\phi_m}^*)B_m = L_{ez}/\omega_c^2 \tag{6}$$

3) Tether and shell vibrations:

$$I_{\Downarrow_n}^*(L'' - u_{po}'' + 3u_{po}) + \sum_m H_{\Downarrow_n\psi_m}^*(A_m'' - 3A_m) - 2\sum_m H_{\psi_n\phi_m}C_m' + (2\alpha' + 2\theta' - 3)H_{x\psi_n}^* + I_{\Downarrow_m}^* h(2\theta' - 3) + \sum_m K_{mn}A_m = H_{ex}^{(n)} \tag{7n}$$

$$\sum_m H_{\phi_n\phi_m}^* C_m'' + 2I_{\phi_n}^*(L' - u'_{po}) + 2\sum_m H_{\phi_n\psi_m}A'_m - H_{x\phi_n}^*(\alpha'' + \theta'' + 3\alpha + 3\theta) - hI_{\phi_n}^*(\theta'' + 3\alpha + 3\theta) + H_{\phi_n\phi_n}\omega_n^2 C_n = H_{ez}^{(n)} \tag{8n}$$

$$\sum_m H_{\phi_n\phi_m}(B_m'' + B_m) + (\gamma'' + 4\gamma - \phi'' - 4\phi)H_{x\phi_n}^* - I_{\phi_n}^*(\phi'' + 4\phi - 3\gamma)h + H_{\phi_n\phi_n}\omega_n^2 B_n = H_{ey}^{(n)} \tag{9n}$$

$$A_{pn}'' + (\omega_n^2/\omega_c^2 - 3)A_{pn} + 2I_1^{(n)}\theta'/M_n = (3I_1^{(n)} + F_{px}\phi_p^o + E_n/\omega_c^2)/M_n \tag{10n}$$

Table 1 Results of calculations for a few modes of the shell

n	(p,j)	λ	ω_n	A_{pj}	C_{pj}	D_{pj}	$I_1^{(n)}$
1	(0, 1)	3.012	1.02778	2.1979	0	−0.08381	2875.55
2	(0, 2)	6.206	1.02946	3.1389	0	3.119e − 3	−322.84
3	(0, 3)	9.371	1.03692	3.8468	0	−1.28e − 4	93.44
4	(0, 4)	12.53	1.05696	4.4425	0	5.368e − 6	−38.73
5	(1, 1)	4.53	1.02821	3.8359	0	−0.019010	0.00
6	(1, 2)	7.737	1.03198	4.9627	0	7.045e − 4	0.00
7	(1, 3)	10.91	1.04459	5.8752	0	−2.845e − 5	0.00
8	(2, 0)	2.292	0.00867	3.6597	−3.47e − 6	0.2240	0.00

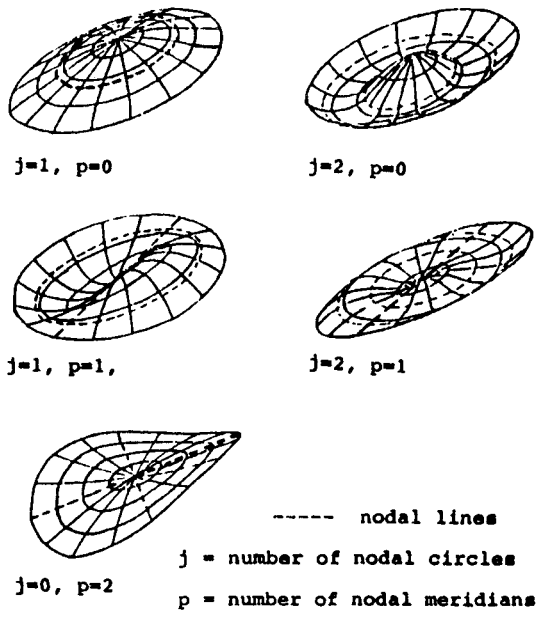

Fig. 2 Several modal shapes of a shell.

Table 2 Degrees of controllability of several actuator designs

Case	No. of actuators	Actuator location	Degree of controllability
1	6		0.0
2	6		1.457×10^{-11}
3	6		0.0
4	12		0.0
5	12		5.893×10^{-11}
6	12	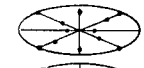	5.443×10^{-9}
7	12	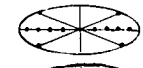	5.443×10^{-9}
8	8	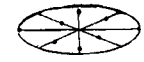	4.987×10^{-9}

It is noted that only the modes without nodal diameters ($p=0$) are coupled to the rotation, so the first four modes ($j=1$, 2, 3, and 4) are considered. For the modes with one nodal diameter ($p=1$) whose amplitudes are quite large during the attiude adjusting, the first three modes ($j=1$, 2, and 3) are included. For the modes without nodal circles ($j=0$), the influence of the shell curvature remains insignificant. Since the frequencies for these modes are very nearly equal to the corresponding flat-plate frequencies, the frequencies are very low. The mode with two nodal diameters is taken as an example. For tether transverse vibration, six modes are taken, three for in plane and three for out-of-plane. The following proposed numerical values of a tethered shell system are adopted here: shell base radius $a=100$ m; shell mass $m_p=10{,}000$ kg; shell curvature radius $R=5$ km; shell height $H=1$ m; shell thickness $h_p=1$ cm; boom length $h=80$ m; shell bending stiffness $D=7.8794*10^5$ N·m; subsatellite mass $m_s=500$ kg; tether mass $m_t=8.35$ kg; commanded tether length $L_c=1$ km; and tether axial stiffness $AE=61{,}645$ N. The deformations of several modes of the shell are shown in Fig. 2, and the results of calculations for a few generic modes are shown in Table 1.

Point Actuator Placement and Model

To control the shape and attitude of the shell and the tether, tether tension alone is not sufficient, and so a few point actuators are added. The concept of the degree of controllability[4] has been used for determinining the placement of the actuators on the shell. The degree of controllability is defined as the minimum eigenvalue of the Grammian form of the controllability matrix and is the scalar measure of system controllability, and its reciprocal indicates the effort to control the system. The values of the degree of controllability for some actuator designs are listed in Table 2. It is assumed that the thrusters at the shell's edge have two jet directions: 1) tangent to the edge, and 2) normal to the shell surface. Each of the other thrusters has only one jet direction, i.e., normal to the shell surface. In case 8 only eight actuators are used, and the degree of controllability is satisfactory, therefore, this actuator location design is recommended.

For an actuator which can generate a force $f_i=(f_x f_y f_z)^T$ and is placed at a location $r_i=(x_i\ y_i\ z_i)^T$, the control torque is given by $r_i\times f_i$, thus in Eqs. (1-3)

$$(L_{epx}\ L_{epy}\ L_{epz})^T=\Sigma r_i\times f_i \tag{11}$$

$$(L_{Epx}\ L_{Epy}\ L_{Epz})^T=(0\ \ C_d\cdot E_{pz}\ \ C_d\cdot E_{py})^T \tag{12}$$

where C_d is the distance between the mass centers of the shell and the tethered shell system. In the remaining equations

$$L_{ey}\approx -I_x E_{pz}/m_\Sigma \tag{13}$$

$$L_{ez}\approx I_{py}E_{py}/m_\Sigma \tag{14}$$

$$H_{ex}^{(n)}=-I_{\psi_n}E_{px}/m_\Sigma \tag{15}$$

$$H_{ey}^{(n)}=-I_{\phi_n}E_{py}/m_\Sigma \tag{16}$$

$$H_{ez}^{(n)}=-I_{\phi_n}E_{pz}/m_\Sigma \tag{17}$$

$$E_n=\sum_{i=1}^{8}\phi_{pn}(y_i,z_i)f_i \tag{18}$$

Attitude and Displacement Sensors

The system will be unobservable if tether transverse motion (swing and vibration) is not measured. The method of measuring tether swing angles by mounting accelerometers on the subsatellite is not suitable, since no attitude control is provided for the subsatellite. A method to measure tether transverse motion is shown in Fig. 3a. The accuracy of the angular transducer can be very high (e.g., transducers used on an inertial platform) during stationkeeping (i.e., the error angle is very small). The subsatellite is quite heavy, so that an inner framed structure is adopted. Since the tether can bear only the longitudinal tension, the position of the frame should coincide with the tangent direction of the tether at the attachment point (Fig. 3b). The displacement of the tether in-plane vibration is approximated by

$$W = \sum_{n=1}^{\infty} C_n(t)\sin(n\pi x/L)$$

then

$$\alpha_1 \approx \tan\alpha_1 = \left.\frac{dW}{dx}\right|_{x=0} = \sum_{n=1}^{\infty} C_n(t)(n\pi/L)\cos(n\pi x/L)|_{x=0}$$

$$= \sum_{n=1}^{\infty} C_n(t)(n\pi/L)$$

The angular transducer A_2 is asumed to measure the in-plane displacement between the shell reference axis and the tether line

$$y_1 = K_\alpha(\alpha+\alpha_1) = K_\alpha\left[\alpha + \sum_{n=1}^{\infty} C_n(t)(n\pi/L)\right] \tag{19}$$

Similarly, for out-of-plane displacement the value obtained from transducer A_1 is

$$y_2 = K_\gamma\left[\gamma + \sum_{n=1}^{\infty} B_n(t)(n\pi/L)\right] \tag{20}$$

A dial with a magnetic encoder is assumed to be used to measure tether length and its changing rate. The dial is fixed to the reel from which the tether is retrieved or deployed. When the dial turns it produces a series of impulses. The sum of the impulse number represents tether length, and the reciprocal of impulse interval represents the rate of tether change.

$$y_3 = K_L L \tag{21}$$

$$y_4 = K_{L'} L' \tag{22}$$

The shell attitude is assumed to be measured by an inertial platform based on gyroscopes. The advantage of the inertial platform is that it produces signals, for both the attitude and angular velocities, with a high signal-to-noise ratio. The drift of the inertial devices is then modified by two infrared horizon sensors of the Earth and two sun sensors.[5] An inertial platform is used because the infrared and sun sensors give signals with low ratios of signal to noise, and in the dark part of the orbit the sun sensor cannot give any signal at all. Consequently, the measurement equations for the shell attitude are

$$y_5 = K_\theta\theta \tag{23}$$

$$y_6 = K_\psi\psi \tag{24}$$

$$y_7 = K_\phi\phi \tag{25}$$

$$y_8 = K_{\theta'}\theta' \tag{26}$$

$$y_9 = K_{\psi'}\psi' \tag{27}$$

$$y_{10} = K_{\phi'}\phi' \tag{28}$$

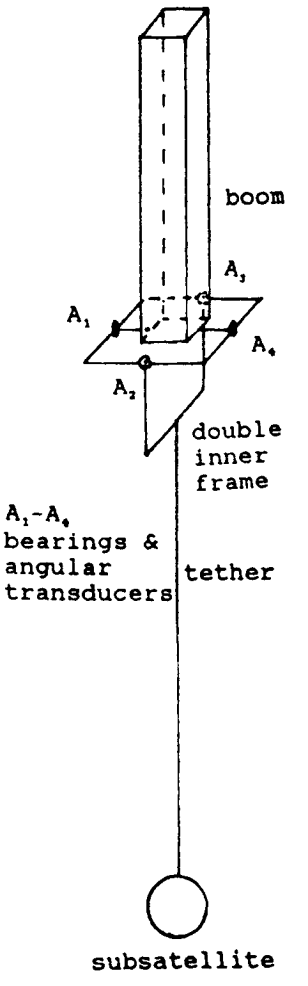

Fig. 3a Design to measure the transverse motion of the tether.

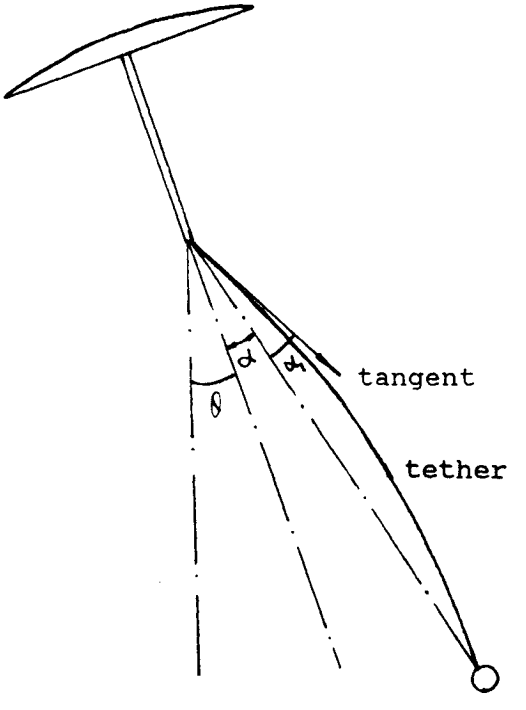

Fig. 3b In-plane angle between the deformed tether and the shell reference.

It is assumed that four displacement sensors, which are collocated with the actuators in the first and second quadrants, are used to measure the shell vibration

$$y_i = K_i \sum_{n=1}^{\infty} \Phi_{pn}(\xi_i \ \zeta_i) A_{p_n}(t) \qquad i = 11, 12, 13, 14 \qquad (29)$$

Equations (19-29) consist of the measurement equations, for which the system is completely observable.

State Equations and Linear Quadratic Gaussian Regulators and Observers

After substituting Eqs. (11-15) into Eqs. (1-10) and after some algebraic manipulations, the system equations can be written in the state vector form

$$x' = Ax + Bu \qquad (30)$$

where

$$u = (f_1, f_2, \ldots, f_8, F_{tx})^T$$

$$x = (\theta, \alpha, L, A_{p_1}, A_{p_2}, \ldots, A_{p_8}, C_1, C_2, C_3, \psi, \phi, \gamma,$$

$$B_1, B_2, B_3, \theta', \alpha', L', A'_{p_1}, A'_{p_2}, \ldots, A_{p_8}, C'_1, C'_2, C'_3,$$

$$\psi', \phi', \gamma', B'_1, B'_2, B'_3)^T$$

In fact, dynamic systems are driven not only by their own control input but also by disturbances which we can neither control nor model deterministically. Sensors generally do not provide exact readings of desired quantities, but introduce their own system dynamics and distortions as well. Furthermore, these devices are also noise corrupted. To meet these difficulties, the LQG techniques are effective. In this section the LQG theory is applied to the design of optimal regulators and estimators for the tethered shell system.

For the infinite-time optimal regulator, given the system represented by Eq. (30), the task is to find the optimal control such that the performance index

$$J = \frac{1}{2} \int_0^{\infty} (x^T Q_c x + u^T R_c u) \, dt \qquad (31)$$

is minimized. In Eq. (31) Q_c is a symmetric positive semidefinite matrix and R_c a symmetric positive definite matrix. After discretization and consideration of noise, Eq. (30) becomes[6]

$$x(k+1) = \tilde{A}(T)x(k) + \tilde{B}(T)u(k) + w(k) \qquad (32)$$

$$y(k) = Cx(k) + v(k) \qquad (33)$$

where

$$\tilde{A}(T) = e^{At} \qquad \tilde{B}(T) = \int_0^T e^{At} B \, dt$$

and Eq. (33) is the state vector form of Eqs. (19-28). The $w(k)$ and $v(k)$ are the n-dimensional and m-dimensional white Gaussian discrete time noise with

$$E[w(i) \ w^T(j)] = Q\delta_{ij} \qquad \text{and} \qquad E[v(i) \ v^T(j)] = R\delta_{ij}$$

respectively, and assumed to be independent of each other and the initial conditions. The initial condition $x(0)$ is modeled as a Gaussian random vector with mean x_0 and covariance P_0.

From Eq. (31), the discretized performance index is[7]

$$J = \lim_{N \to \infty} \frac{1}{N} E\left\{ \sum_{k=0}^{N-1} [x^T(k+1)\tilde{Q}x(k+1) + 2x^T(k+1)\tilde{W}u(k) + u^T(k)\tilde{R}u(k)] \right\} \qquad (34)$$

Table 3 Maximum and minimum moduli of eigenvalues of the Kalman filter

μ_Q	Minimum	Maximum
10^{-11}	$6.3514e-4$	0.96714
10^{-12}	$1.6817e-2$	0.97003
10^{-14}	0.11649	0.97714
10^{-16}	0.55691	0.98687

Table 4 Maximum and minimum moduli of eigenvalues of the regulator

μ_C	Minimum	Maximum
10^{-3}	0.88481	0.99948
10^{-4}	0.83930	0.99943
10^{-6}	0.73230	0.99850
10^{-7}	0.57579	0.99701

where

$$\tilde{Q} = \int_0^T e^{A^T t} Q_c e^{At} \, dt \qquad \tilde{W} = \int_0^T e^{A^T t} Q_c g(t,0) \, dt$$

$$\tilde{R} = \int_0^T [R_c + g^T(t,0) Q_c g(t,0) \, dt$$

$$g(t,0) = \int_0^t e^{As} B \, ds$$

If the system represented by Eqs. (32) and (33) is controllable (or stabilizable) and observable (detectable), the LQG solution is[8,9]

$$u(k) = -G\hat{x}(k) \qquad (35)$$

$$G = -(\tilde{R} + \tilde{B}^T P \tilde{B})^{-1}(\tilde{B}^T P \tilde{A} + \tilde{W}^T) \qquad (36)$$

where P satisfies the algebraic Riccati equation

$$P = \tilde{A}^T P \tilde{A} + \tilde{Q} - (\tilde{A}^T P \tilde{B} + \tilde{W})(\tilde{R} + \tilde{B}^T P \tilde{B})^{-1}(\tilde{B}^T P \tilde{A} + \tilde{W}^T) \qquad (37)$$

The state estimate at the kth interval can be related to its predicted value based on information from the $(k-1)$ interval, together with the measurement vector at the kth interval, as

$$\hat{x}(k) = \hat{x}(k/k-1) + K[y(k) - C\hat{x}(k/k-1)] \qquad (38)$$

$$\hat{x}(k/k-1) = \tilde{A}\hat{x}(k-1) + \tilde{B}u(k-1) \qquad (39)$$

$$K = P_e C^T (C P_e C^T + R)^{-1} \qquad (40)$$

The covariance of the state estimate P_e satisfies the algebraic Riccati equation

$$P_e = (\tilde{A} - K^* C) P_e (\tilde{A} - K^* C)^T + K^* R K^{*T} + Q \qquad (41)$$

where $K^* = \tilde{A}K$.

As a result of computational delay, what is often considered for implementation is not the control law given by Eq. (35), but a control

$$u(k) = -G\hat{x}(k/k-1) \qquad (42)$$

The LQG control dynamics consist of two parts: the dynamics of the plant with a feedback controller and the dynamics of the estimator feedback loop. The matrices describing the dynamics of the closed-loop controller and the closed-loop estimator, respectively, are

$$A_c^* = \tilde{A} - \tilde{B}G \tag{43}$$

$$A_e^* = \tilde{A} - K^*C \tag{44}$$

It has been shown that the eigenvalues of A_c^* and A_e^* are independent of each other.[10] Therefore, in the synthesis it is possible to arrange the poles of the estimators and controllers separately.

It is well known that if and only if the open-loop system model is both stabilizable and detectable, there exist gains G and K^* that can provide asymptotic closed-loop stability. Furthermore, under the stronger assumptions of complete controllability and complete observability (as in the designs of the actuators and measurements for the tethered shell system, here), we can place both the regulator and observer poles arbitrarily (within the restriction of the complex conjugate pairs).

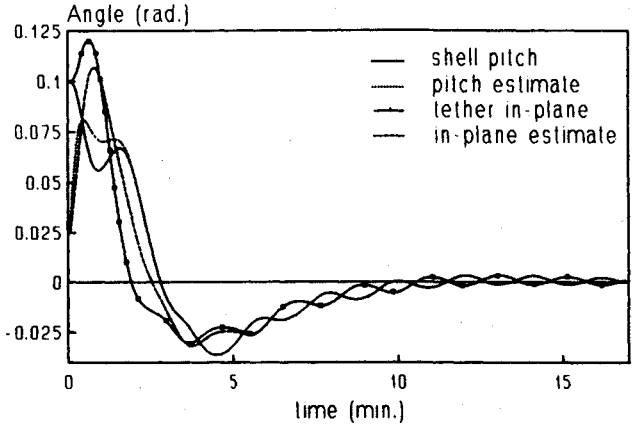

Fig. 4a Shell pitch and tether in-plane swing.

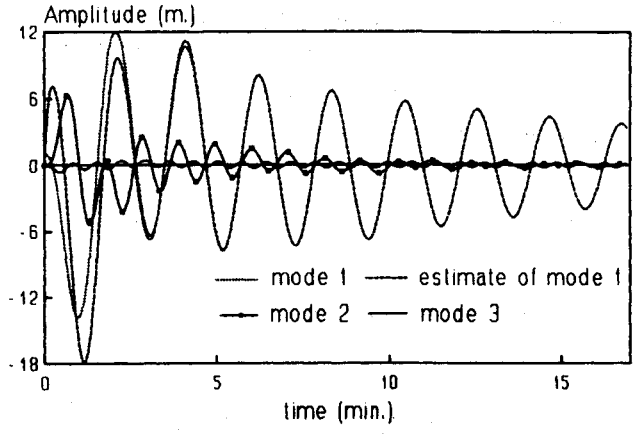

Fig. 4b Tether in-plane transverse vibrations.

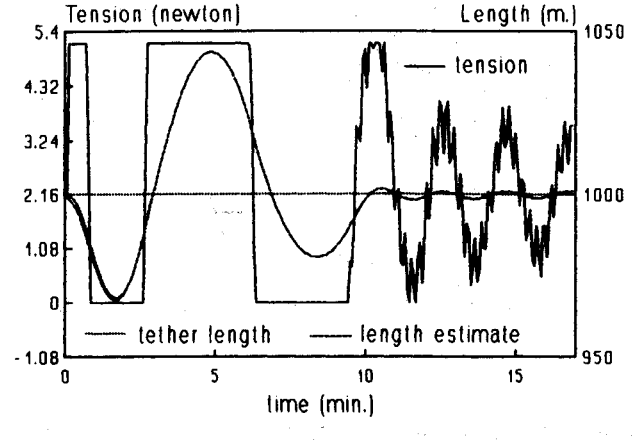

Fig. 4c Tether tension and length.

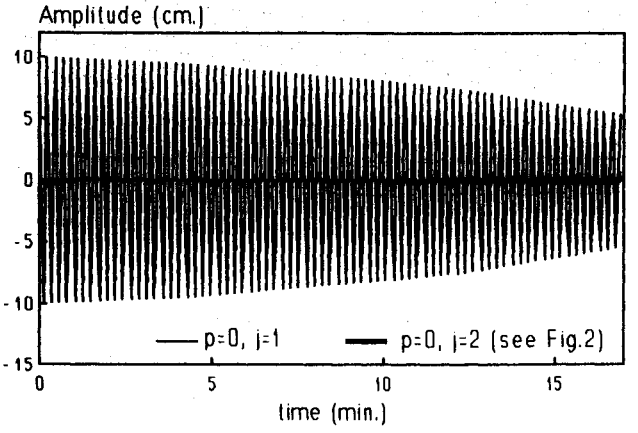

Fig. 4d Shell axisymmetric modes.

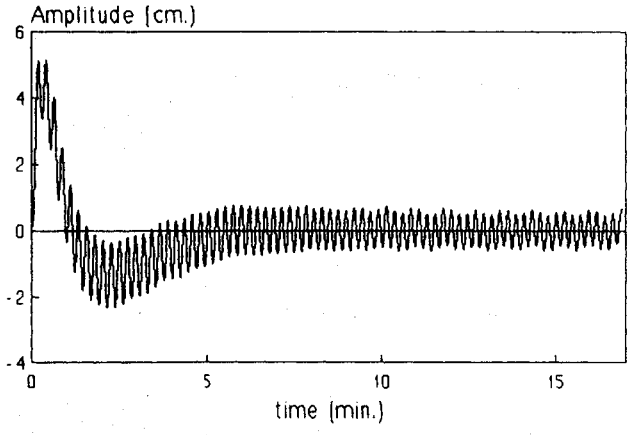

Fig. 4e Shell mode; $p = 1, j = 1$, see Fig. 2.

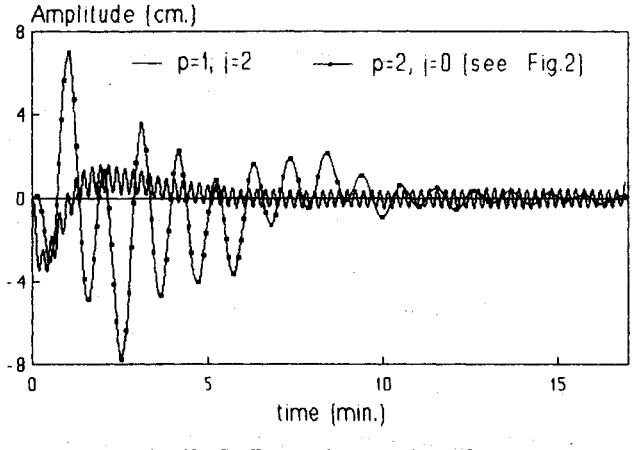

Fig. 4f Shell nonaxisymmetric modes.

It should be noted that in Eq. (30) the differentials are with respect to the orbit time, i.e.,

$$x_i' = \frac{dx_i}{d\omega_c t} = \left(\frac{1}{\omega_c}\right)\frac{dx_i}{dt}$$

If the noise added to dx_i/dt is w_i, the noise added to x_i' should be $(1/\omega_c)w_i$, and so the covariance matrices should be[11]

$$Q = \mu_Q \begin{bmatrix} I_{20} & 0 \\ 0 & (1/\omega_c^2)I_{20} \end{bmatrix} \qquad R = \mu_R \begin{bmatrix} I_{10} & 0 \\ 0 & (1/\omega_c^2)I_4 \end{bmatrix} \tag{45}$$

For the control loop let the weighting matrices

$$Q_C = C^T C \qquad R_c = \mu_C I$$

To find the appropriate arrangement of the observer and controller poles it is necessary to study the loci of the eigenvalues of A_e^* and A_c^* with μ_Q, μ_R, and μ_C, respectively. The maximum and minimum moduli of the eigenvalues of A_e^* and A_c^* vs the different parameters μ_Q, μ_R, and μ_C are listed in Tables 3 and 4, respectively. Based on the data in Tables 3 and 4 we can arrange the position of the controller and observer poles.

Simulations

It is assumed that the accuracy of the displacement sensors is about 1 cm for the shell deflection, the angular sensor accuracy is about 10^{-4} rad, and the modeling error for the dynamical system is less than the error of the measurement sensors. In Eq. (45) the parameters of the covariance matrices used for simulation are $\mu_R = 10^{-8}$ and $\mu_Q = 10^{-16}$. It is also assumed that both the measurement and the plant noises are Gaussian white noises with zero mean.

The initial state is also assumed to be noise corrupted

$$x(0) = x_0 + w_0 \qquad x_0 = E\{x(0)\} \qquad P_o = E\{w_0 w_0^T\}$$

The initial conditions are assumed as: $\theta(0) = 0.1$ rad, $\alpha(0) = 0.1$ rad, $L(0) = 1001$ m, $A_{P_1}(0) = 0.1$ m, $C_1(0) = 1$ m, $\psi(0) = 0.1$ rad, $\phi(0) = 0.1$ rad, $\gamma(0) = 0.1$ rad, and $B_1(0) = 1$ m; and the rest of the initial conditions are taken to be zero. The initial values of the estimated state are assumed to be zero, i.e., $x_i(0/-1) = 0.0$ $(i = 1, 2, \ldots, 40)$.

The strategy of choosing the sampling time T should be to select the sampling time as long as possible after the performance of the sampled-data system meets the requirements of the design. Generally speaking, too long a sampling interval tends to deteriorate the performance of a sampled-data system (increase the sensitivity, decrease stability, loss of controllability, etc.).[11] On the other hand, the implementation of a very short sampling interval may be limited by computer operation times and the expense of fast analog-to-digital and digital-to-analog devices. The choice of the sampling time T will also be constrained by the capability to restore the signal that comes from observational data, i.e., T meets Shannon's theorem, $T < \pi/\omega_m$, where ω_m is the maximum frequency of the input signal. In the simulation here, $T = 3$ s.

In general, as for the design of the Kalman filter, the considered covariances of the measurement and plant noises should be greater than or equal to the actual ones. After these conditions have been satisfied the location of the observer poles may be changed by means of the variation of the parameters μ_R and μ_Q. As we know, the minimum and maximum moduli of the observer closed-loop eigenvalues should be less than those of the controller closed-loop eigenvalues so that the estimator can provide accurate, timely state information for the controller. Based on this principle, every combination in Tables 3 and 4 is simulated and it is found that if the observer converges too fast the system will be very sensitive to the noise. So the possible appropriate minimum and maximum moduli of controller eigenvalues are 0.57579 and 0.99701, whereas the corresponding ones of the observer's are 0.55691 and 0.98687.

The typical results of the simulations are shown in Figs. 4–6. Figure 4 is for the in-plane motion, Fig. 5 for the out-of-plane motion, and Fig. 6 for each actuator force needed during the regulating process.

Since the tether cannot support compressive forces and a large tension force should be avoided, the tether tension boundary is set as $0 < F_{tx} < 5$ N (Fig. 4c). The result of the simulation is satisfactory. The initial errors are converging smoothly, and the required forces for each actuator are reasonable. After 5 min we can hardly see any difference between the actual value of each state variable and its estimate. Other

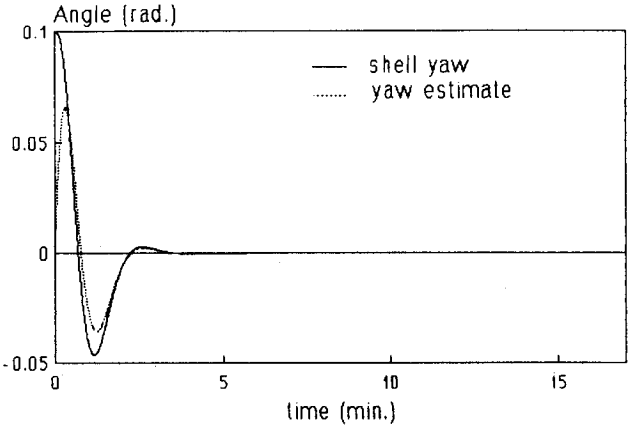

Fig. 5a Shell yaw angle.

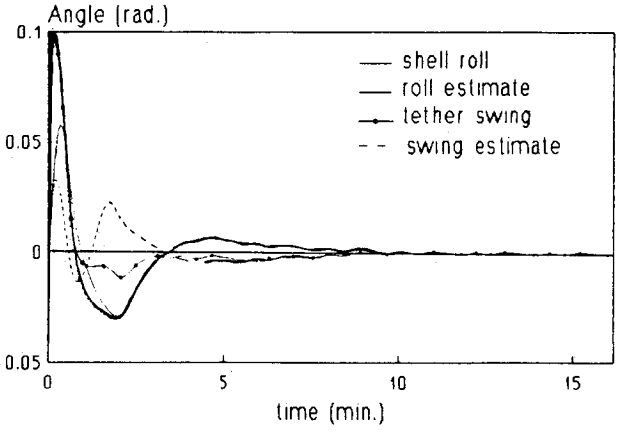

Fig. 5b Shell roll and tether out-of-plane swing.

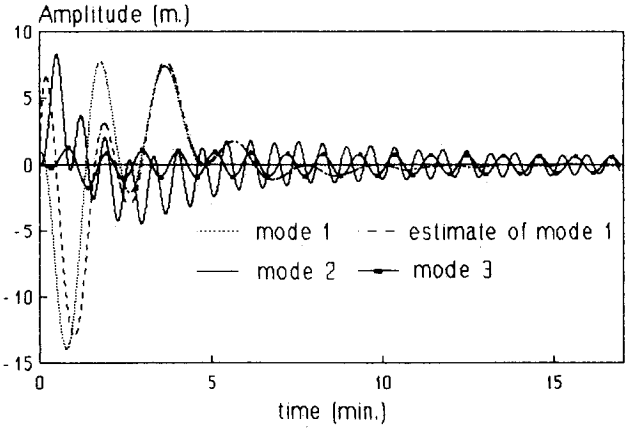

Fig. 5c Tether out-of-plane vibrations.

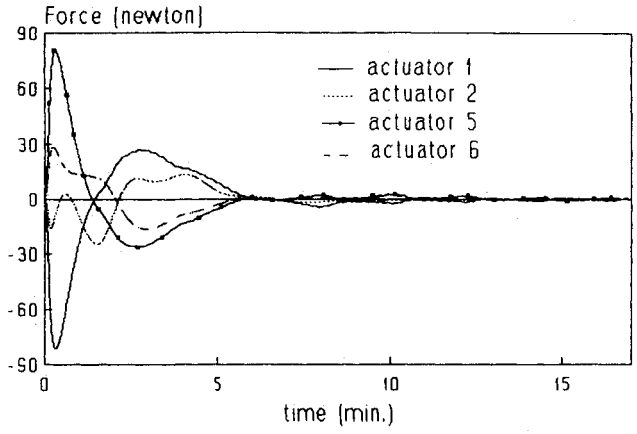

Fig. 6 Transient response of several actuators.

simulation results based on the parameters of Table 3 and 4, as well as with different initial conditions, lead to results similar to those shown here.

Conclusions

1) The actuator placement design used here is satisfactory. The degree of controllability is quite high considering only eight point actuators are applied. This design can control elastic vibrations and orientations of a flexible shell and a flexible tether, and it has been verified by simulations.

2) The system is not observable if the tether transverse motions are not directly measured. The method of measuring tether transverse motion can be applied not only to tethered shell systems, but also to any system with a tether. This design is easy to implement in engineering practice.

3) The discrete time data system is more practical for a controller based on an on-board computer system. The sampling time of $T = 3$ s is a good compromise between the performance of the system and the capacity of the on-board computer.

4) For a dynamic system with plant and measurement noise, the LQG technique is effective. As for the placement of the controller and observer poles, the minimum and the maximum moduli of the eigenvalues of the closed-loop observer must be less than the minimum and maximum moduli of the eigenvalues of the closed-loop controller, respectively, so that the observer can provide the timely and accurate estimate of the state variables for the controller. We should also ensure that the ratio μ_R/μ_Q cannot be too small, otherwise the Kalman filter may become too sensitive to the observation noise.

5) Since the tethered shell system consists of a flexible shell and flexible tether, the dimensionality of the state vector is as high as 40. Because of the practical possibility of on-board computational implementation, it is suggested that further research be performed on design of low-order controllers based on robustness theory.

Acknowledgments

This work was supported by the Air Force Office of Scientific Research, under Contract F49620-90-C-009, with Spencer Wu as the Program Manager. The authors thank Suresh M. Joshi for his valuable remarks and suggestions related to this paper. The authors also wish to express their gratitude for the valuable remarks and suggestions made by the reviewers.

References

[1]Liu, L., and Bainum, P. M., "Effect of Tether Flexibility on Tethered Shuttle Subsatellite Stability and Control," PSN/NASA/AIDAA Second International Conference on Tethers in Space, Venice, Italy, Oct. 4-8, 1987; also *Journal of Guidance, Control, and Dynamics,* Vol. 12, No. 6, 1989, pp. 866-873.

[2]Tan, Z., and Bainum, P. M., "Minimum-Time Large Angle Slew of an Orbiting Flexible Shallow Spherical Shell System," First Annual AAS/AIAA Space Flight Mechanics Conf., AAS 91-144, Houston, TX, Feb. 11-13, 1991.

[3]Liu, L., and Bainum, P. M., "Dynamics and Control of Tethered Antennas/Reflectors in Orbit," Third International Conf. on Tethers in Space, San Francisco, CA, May 17-19, 1989; also *Journal of the Astronautical Sciences,* Vol. 38, No. 3, 1990, pp. 247-268.

[4]Xing, G., and Bainum, P. M., "Some Definitions of Degree of Controllability (Observability) for Discrete-Time System and their Applications," 12th Biennial American Society of Mechanical Engineers Conf. on Mechanical Vibrations and Noise, Montreal, Canada, Sept. 17-20, 1989; also "Actuator Placement Using Degree of Controllability for Discrete-Time Systems," *Transactions of the ASME, Journal of Dynamic Systems, Measurement, and Control,* Vol. 114, Sept. 1992, pp. 508-516.

[5]Xing, G., and Bainum, P. M., "The Optimal LQG Digital Shape and Orientation Control of an Orbiting Shallow Spherical Shell System," 40th Congress of the International Astronautical Federation, Beijing, China, Oct. 7-12, 1989; also *Acta Astronatica,* Vol. 21, No. 10, 1990, pp. 719-731.

[6]Kuo, B. C., "Design of Digital Control Systems with State Feedback and Dynamics Output Feedback," *Journal of the Astronautical Sciences,* Vol. 27, No. 2, 1979, pp. 207-214.

[7]Armstrong, E. S., *ORACLS, A Design System for Linear Multivariable Control,* Marcel Dekker, New York, 1980, pp. 83-87.

[8]Kwakernaak, H., and Sivan, R., *Linear Optimal Control Systems,* Wiley, New York, 1982, pp. 488-536.

[9]Maybeck, P. S., *Stochastic Models, Estimation and Control,* Vol. 3, Academic Press, New York, 1982.

[10]Xing, G., and Bainum, P. M., "The Optimal LQG Control of Orbiting Large Flexible Beams," *Journal of the Astronautical Sciences,* Vol. 37, No. 1, 1989, pp. 59-78.

[11]Tan, Z., and Bainum, P. M., "The Optimal LQG Digital Control of An Orbiting Large Flexible Platform," *Proceedings of the International Conf. on Dynamics, Vibration and Control,* edited by W. Zhaolin, Peking Univ. Press, Beijing, China, 1990, pp. 179-193.